Research Article

Journal of Environmental Nanotechnology

Electropolymerized Poly(4-amino-1,2,4-triazole) with Inorganic Oxides as Advanced Corrosion-Inhibitive Coatings for Cu–Ni (90/10) Alloy

T. Srinivasan[1], J. Balaji[2] and M. G. Sethuraman[3*]

[1]Department of Chemistry, G.T.N. Arts College (Autonomous), Dindigul, TN, India
[2]Department of Chemistry, National College (Autonomous), Tiruchirappalli, TN, India
[3]Department of Chemistry, The Gandhigram Rural Institute (Deemed to be University), Gandhigram, TN, India
Received: 13.10.2025 Accepted: 26.01.2026 Published: 30.03.2026
*mgsethu@rediffmail.com

ABSTRACT

The present study focuses on the electrochemical synthesis and characterization of poly(4-amino-1,2,4-triazole) (poly-4-ATA) and its composites incorporating various metal oxides. Metal oxides such as CeO_2, ZnO, and TiO_2, along with SiO_2, were integrated into the polymer matrix to enhance the structural, morphological, and electrochemical performance of the coatings. The prepared materials were examined by FT-IR, XRD, SEM, EDAX, and electrochemical analyses, confirming successful polymerization and the uniform distribution of metal oxide particles within the polymer network. Electrochemical investigations, including potentiodynamic polarization (PP) and electrochemical impedance spectroscopy (EIS), revealed that The incorporation of TiO_2 of metal oxides significantly improved corrosion resistance compared with that of the bare alloy and the pure polymer film. Among the tested composites, the poly-4-ATA/TiO_2 coating exhibited the highest charge-transfer resistance and an inhibition efficiency of 97.8%, indicating superior protective performance. These findings suggest that poly-4-ATA/metal oxide composites are promising corrosion-inhibitive coatings, with the synergistic effect of the polymer and the metal oxide contributing to the enhanced durability and stability of metallic substrates in aggressive chloride environments.

Keywords: Poly(4-amino-1,2,4-triazole); Cu–Ni alloy; Corrosion inhibition; Electropolymerization: Inorganic oxides.

1. INTRODUCTION

Corrosion poses a significant threat to critical infrastructure, such as bridges, pipelines, and buildings. It weakens the structural integrity of these constructions, potentially leading to catastrophic failures. The economic impact of corrosion is significant. Maintenance, repairs, and replacements of corroded infrastructure cost billions of dollars annually. Industries like transportation, oil, energy, and manufacturing are particularly vulnerable to these financial losses. Structural corrosion can compromise public safety. From rusted support beams in buildings to corroded sections of highways, the risk of accidents and injuries increases significantly. Leaks in corroded pipelines can result in the release of hazardous substances into the environment, leading to pollution and ecosystem damage. Corrosion also affects electronic devices, leading to malfunctions and reduced lifespans. This is particularly concerning given the increasing reliance on technology in the modern world (Aslam *et al*. 2022).

Corrosion refers to a broad range of material degradation phenomena, governed by distinct electrochemical, environmental, mechanical, and biological conditions. It is a complex and dynamic interaction between a metal or alloy and its environment. Material degradation eventually leads to loss of material, functionality, and mechanical integrity over time. Unlike the general presumption that metals corrode uniformly, actual engineering systems tend to undergo localized or non-uniform corrosion, which can be more hazardous as it goes on unnoticed until the event of critical failure.

The nature, extent, and severity of the corrosion are heavily dependent on an interplay of factors, such as the chemical composition of the metal, surface conditions, the character of the electrolyte, temperature, and the presence of microorganisms. Hence, a customized method is needed depending on the prevalent corrosion mechanism in the environment (Aydin, 2023).

The deterioration of metals due to corrosion is a serious concern across industries. It is affecting the longevity, safety, and performance of the equipment. While physical and chemical coatings offer some degree of protection, one of the most economical and widely adopted strategies to combat corrosion is the use of corrosion inhibitors. These substances, when added in small amounts to a corrosive medium, significantly reduce the rate of metal degradation by interfering with the electrochemical reactions responsible for corrosion (Winkler *et al*. 2025).

Corrosion inhibitors are especially valuable in processes involving acid cleaning, pickling, cooling water circulation, oil and gas production, and closed-loop systems, where metals are continuously exposed to aggressive environments. Their action is generally based on the formation of a protective film on the metal surface, which acts as a barrier to corrosive ions such as hydrogen ions (H^+), oxygen (O), and chlorides (Cl^-). Given the wide range of operating environments and metal types, corrosion inhibitors are broadly classified based on their mechanism of action, chemical composition, and source of origin (Aslam *et al*. 2022).

Corrosion of metals is a widespread and critical issue impacting a broad range of industries, including transportation, infrastructure, marine, oil and gas, and manufacturing. This degradation process occurs when metals react with environmental agents such as water, oxygen, acids, and industrial chemicals, leading to material weakening, structural failure, production downtime, and significant financial losses. To combat this challenge, various preventive strategies have been developed, among which the use of chemical corrosion inhibitors remains one of the most practical and cost-effective solutions. These inhibitors are added in small quantities to corrosive media to significantly slow down the corrosion rate without requiring major changes to the process environment or operational conditions (Vinothkumar and Sethuraman, 2020).

With growing concerns over environmental safety and sustainability, the focus has increasingly shifted towards the development of organic inhibitors that are both effective and eco-friendly. Among these, heterocyclic compounds have gained prominence due to their ability to form stable interactions with metal surfaces. Particularly, triazole-based inhibitors have garnered significant attention for their superior performance. Triazoles are five-membered heterocycles rich in nitrogen, typically containing three nitrogen atoms within the ring. This high nitrogen content facilitates strong adsorption onto the metal surface through lone pair donation and π-electron interactions, leading to the formation of protective films that hinder both anodic and cathodic corrosion reactions (Rajkumar and Sethuraman, 2014; Phadke *et al*. 2017).

Moreover, the triazole framework is highly tunable. The introduction of various substituent groups such as amino ($–NH_2$) and thiol (–SH) can enhance the electron-donating ability of the molecule, increase its solubility, and improve its overall adsorption characteristics. These modifications allow for tailoring of the inhibitor's electronic and steric properties, enabling targeted interaction with specific metal surfaces and adaptability to different corrosive environments (Akpan *et al*. 2024).

Mohanty *et al.* (2021) investigated how structural modification of triazole-based inhibitors can enhance their corrosion protection. The weak inhibitor 4-amino-1,2,4-triazole (AT) was functionalized with an octanoyl group to produce N-(4H-1,2,4-triazol-4-yl) octanamide (OAT). Electrochemical and gravimetric studies revealed that this modification converted the adsorption mechanism from physisorption to chemisorption, improving inhibition efficiency from around 65% for AT (10 mM) to more than 99% for OAT at significantly lower concentrations (0.3–0.5 mM). OAT retained high protective performance across a wide temperature range (30–60 °C). XPS analysis confirmed chemisorption through triazole nitrogen atoms, while EIS, SECM (scanning electrochemical microscopy), and SEM analysis confirmed the formation of a uniform self-assembled monolayer (SAM) that effectively shielded mild steel from corrosion in 0.1 M HCl. These results emphasize that targeted chemical modification of triazole molecules can produce highly effective and thermally stable corrosion inhibitors (Mohanty *et al.* 2021).

In this present research work, the prepared poly-4-ATA material exhibits significant anticorrosive properties by forming a protective polymeric layer on the Cu–Ni (90/10) alloy surface, which restricts the interaction between the metal substrate and the 3.5% NaCl as aelectrolyte medium. However, the inhibition capability of the polymer alone can be further strengthened through the incorporation of selected metal oxides such as SiO_2, CeO_2, ZnO, and TiO_2, respectively. The presence of these metal oxide particles not only improves the barrier characteristics of the polymeric coating but also enhances surface coverage, mechanical stability, and charge-transfer resistance. These oxides act synergistically with the poly-4-ATA matrix, leading to reduced porosity, improved adherence to the metal surface, and better blocking of corrosive ions. As a result, the hybrid poly-4-ATA/metal oxide films provide superior protection efficiency compared to the pristine polymer film.

2. MATERIALS AND METHODS

The supplementary material provides information about the chemicals used and the characterization of the synthesized polymer/metal oxide composites. All reagents were of analytical grade and applied without further purification, with their specifications listed in the supplementary data. The composites were analyzed for structural, morphological, thermal, and elemental features using FT-IR, XRD, and SEM/EDAX techniques. In addition, their electrochemical performance was evaluated through cyclic voltammetry, electrochemical impedance spectroscopy, and the potentiodynamic polarization technique.

2.1 Electropolymerization of 4-Amino-1,2,4-Triazole (4-ATA)

The Cu–Ni (90/10) alloy electrode was immersed in an electrolyte solution composed of 0.1 M 4-ATA dissolved in methanol and 0.5 M NaOH, which acted both as a supporting electrolyte and as a medium for the polymerization reaction. To prepare the composite coatings, 0.1 M 4-ATA was dissolved in methanol and mixed with 0.5 M NaOH, after which 1 mM of TiO_2, ZnO, CeO_2, or SiO_2 particles were introduced into individual beakers. Since metal oxide particles tend to aggregate, the suspensions were subjected to ultrasonic irradiation for about 30 minutes to achieve uniform dispersion of the particles within the electrolyte solution.

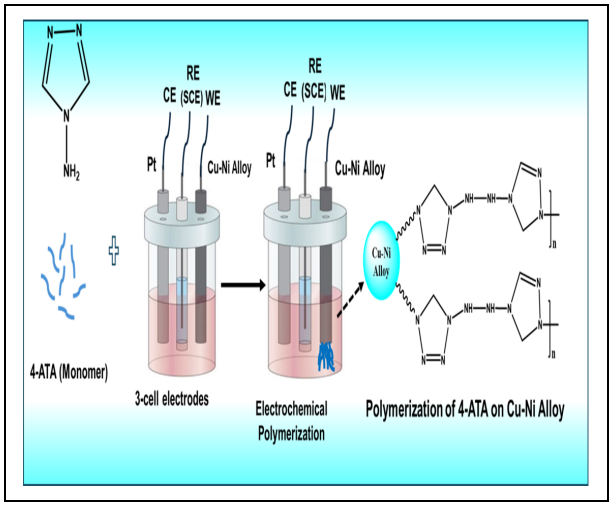


Fig. 1: Schematic representation of poly-4-ATA formation

Following the electrodeposition process (Fig. 1), the Cu–Ni (90/10) alloy electrodes modified with poly-4-ATA or poly-4-ATA/metal oxide composites were carefully removed from the electrochemical cell. To eliminate any loosely adhered or physically adsorbed residues, the coated electrodes were thoroughly rinsed with double-distilled water. Finally, the electrodes were dried in an oven at 65 °C to remove moisture and stabilize the polymer/oxide composite layers, after which they were subjected to subsequent structural, morphological, and electrochemical studies.

3. RESULTS AND DISCUSSION

3.1. Cyclic Voltammetric Studies of Poly-4-ATA and its Metal Oxide Composites

Cyclic voltammograms of poly-4-ATA and its metal oxide composites are depicted in Figs. 2a–2e. The anodic current increases may confirm the electropolymerization process, which occurred on the electrode surface with the incorporation of various metal oxides. After several cycles, the metal oxide enhanced the current response, while the poly-4-ATA/TiO_2 composite showed the greatest effect (Fig. 2e) (Ates *et al.* 2015). The coating thicknesses were 4.12 µm for pure poly-4-ATA and 3.68 µm for composites.

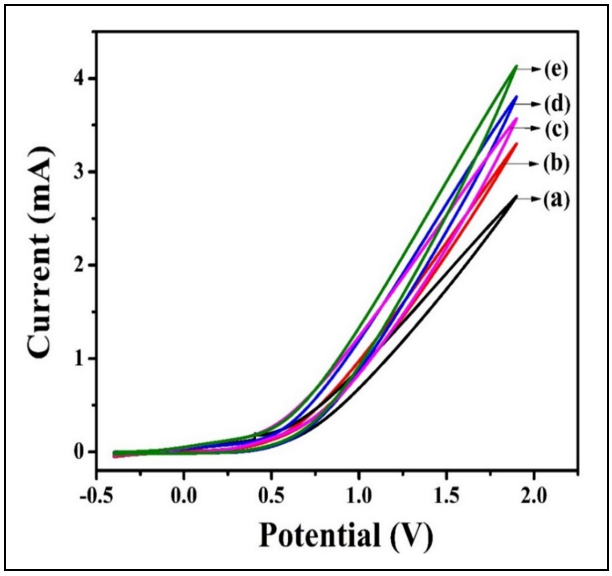


Fig. 2: Cyclic voltammograms of (a) poly-4-ATA, (b) poly-4-ATA/SiO_2, (c) poly-4-ATA/CeO_2, (d) poly-4-ATA/ZnO, and (e) poly-4-ATA/TiO_2

3.2 FT-IR Studies of Poly-4-ATA and its Metal Oxide Composites

The FT-IR spectra of poly-4-ATA and its metal oxide composites are shown in Figs. 3a–3e, and the spectral values are tabulated in Table 1.

The observed major vibrational features are associated with the polymer backbone as well as the characteristic signals of the incorporated oxides. A broad absorption band in the range of 3404–3438 cm^{-1} corresponds to N–H stretching, while a distinct band around 2920–2926 cm^{-1} is attributed to aromatic C–H stretching (Rajkumar and Sethuraman, 2015). The presence of these absorptions confirms the retention of the triazole ring structure within the polymer after electropolymerization.

The band within the range of 1620–1630 cm^{-1} is associated with the bending vibration of the N–H group, which appears in both the poly-4-ATA and its metal oxide composites (Rajkumar and Sethuraman, 2015). Another characteristic band detected in the region of 1380–1411 cm^{-1} corresponds to the stretching vibration of the C–N bond, confirming the structural features of poly-4-ATA and its oxide composites (Vinothkumar and Sethuraman, 2018). The spectral band detected between 1038–1049 cm^{-1} corresponds to the C–C stretching vibration of the polymer backbone (Edison *et al.* 2018). This feature is consistently

observed in poly-4-ATA and remains when metal oxides are incorporated into the polymer matrix, indicating the retention of the main chain structure.

Table 1. FT-IR spectral values of poly-4-ATA and its metal oxide composites

S. No.	Wavenumber (cm^{-1})					Band Assignment
	Poly 4-ATA	Poly-4-ATA/SiO_2	Poly-4-ATA/CeO_2	Poly-4-ATA/ZnO	Poly-4-ATA/TiO_2	
1	3411	3422	3404	3404	3438	N-H stretching
2	2920	2926	2926	2923	2926	Aromatic C-H stretching
3	1620	1630	1625	1621	1620	N-H bending vibration
4	1380	1411	1387	1393	1400	C-N stretching
5	1043	1038	1049	1049	1038	-C-C stretching
6	-	-	-	553	-	Zn-O stretching
7	-	-	540	-	-	Ce-O stretching
8	-	1099	-	-	-	Si-O-Si stretching
9	-	-	-	-	571	Ti-O stretching

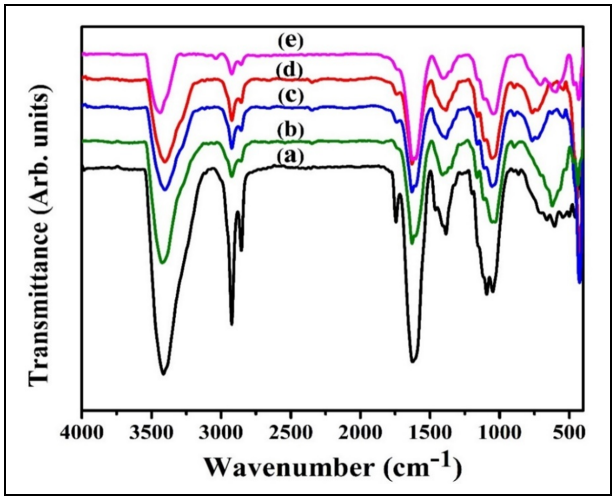


Fig. 3: Comparison of FT-IR spectra of (a) poly 4-ATA, (b) poly-4-ATA/SiO_2, (c) poly-4-ATA/CeO_2, (d) poly-4-ATA/ZnO, and (e) poly-4-ATA/TiO_2

In addition to the polymer-related vibrations, oxide-specific peaks appear in the composite samples. A band near 553 cm^{-1} is assigned to Zn–O stretching (Li *et al.* 2019), while Ce–O vibrations are observed around 540 cm^{-1} (Hosseini and Aboutalebi, 2019). The asymmetric stretching of Si–O–Si networks is evident at 1099 cm^{-1} (Saravanan and Dubey, 2020), and Ti–O stretching vibration emerges near 571 cm^{-1} (Elangovan *et al.* 2024). These bands, which are absent in the pure poly-4-ATA spectrum, confirm the successful incorporation of the respective metal oxides into the polymer matrix.

It is also noteworthy that the N–H stretching frequency exhibits slight shifts (±3 cm^{-1}) compared to the undoped polymer. Such subtle changes are often indicative of weak interactions between the polymer chains and the oxide nanoparticles. In this case, the shifts can be rationalized by hydrogen bonding or surface coordination between oxide hydroxyl groups (such as Ti–OH or Si–OH) and the N–H sites of the polymer. These interfacial interactions not only validate the effective integration of oxides into the polymer framework but may also influence the electronic, structural, and electrochemical properties of the resulting composites.

3.3 XRD Pattern of Poly-4-ATA and its Metal Oxide Composites

The XRD profiles of poly-4-ATA and its oxide composites (poly-4-ATA/CeO_2, poly-4-ATA/SiO_2, poly-4-ATA/ZnO and poly-4-ATA/TiO_2) are presented in Figs. 4a–4e, and the corresponding 2θ values are listed in Table 2.

Table 2. 2θ values of poly-4-ATA and its metal oxide composites

S. No.	Poly 4-ATA	Poly 4-ATA/CeO_2	Poly 4-ATA/SiO_2	Poly 4-ATA/ZnO	Poly 4-ATA/TiO_2
1	23.59	23.47	23.37	23.47	23.47
2	27.17	27.04	26.92	27.04	27.04
3	38.62	38.62	38.62	38.49	38.68
4	45.65	45.65	45.65	45.52	45.59
5	47.80	47.92	47.92	47.80	47.80
6	55.92	55.67	55.92	55.79	55.79
7	61.39	61.14	61.27	62.95	61.39
8	63.20	63.07	63.07	-	63.07
9	69.98	69.85	69.98	69.85	69.73
10	75.11	74.86	74.86	74.80	74.86
JCPDS Card No.	-	340394	897499	891397	896975

The poly-4-ATA (Fig. 4a) shows sharp diffraction peaks at 23.59, 27.17, 38.62, 45.65, 47.80, 55.92, 61.39, 63.20, 69.98, and 75.11°, characteristic of an amorphous or semi-crystalline structure. The reduced crystallinity can be attributed to the amino substituent of the 4-ATA monomer, which disrupts chain packing and lowers long-range order.

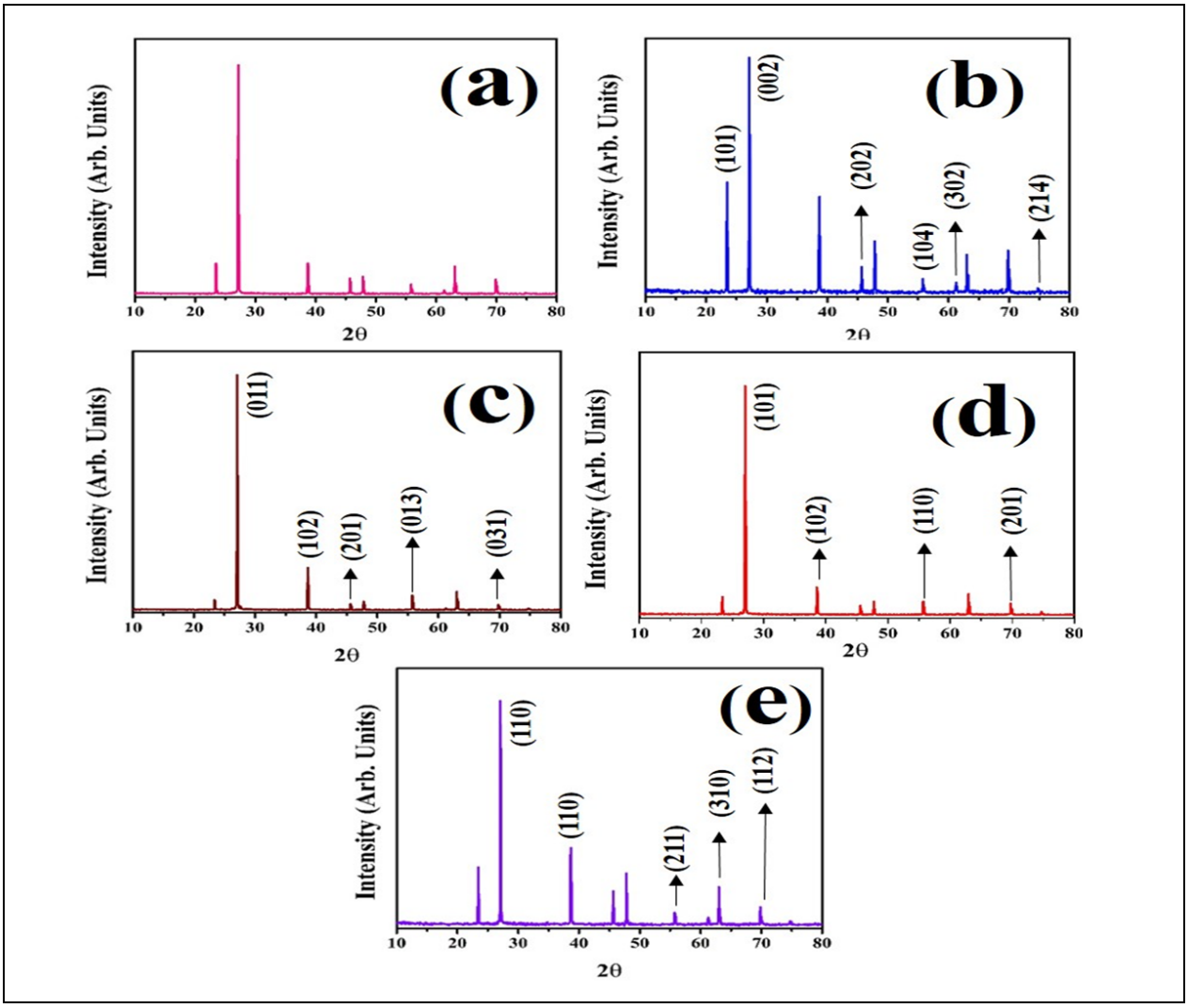


Fig. 4: XRD patterns of (a) poly 4-ATA, (b) poly-4-ATA/CeO_2, (c) poly-4-ATA/SiO_2, (d) poly-4-ATA/ZnO and (e) poly-4-ATA/TiO_2

For the poly-4-ATA/CeO_2 composite (Fig. 4b), peaks appeared at 23.47, 27.04, 38.62, 45.65, 47.92, 55.67, 61.14, 63.07, 69.85, and 74.86°. The shift of the 2θ value from 23.59° (in the pure polymer) to 23.47° suggests lattice strain introduced by CeO_2 nanoparticles, causing local stress and minor rearrangements in the polymer framework (JCPDS: 34-0394) (Choudhury and Choudhury, 2012).

In the case of poly-4-ATA/SiO_2 (Fig. 4c), the XRD pattern showed peaks at 23.37, 26.92, 38.62, 45.65, 47.92, 55.92, 61.27, 63.07, 69.98, and 74.86°, which were slightly shifted relative to the pure polymer. This indicates that SiO_2 incorporation leads to lattice distortion and interplanar spacing variations. The pattern matches JCPDS card 89-7499, confirming successful integration of SiO_2 in an amorphous semi-crystalline form (Singh *et al.* 2019). Such lattice strain is significant, as it can affect charge transport, structural stability, and electrochemical behaviour.

For the poly-4-ATA/ZnO composite (Fig. 4d), diffraction peaks were observed at 23.47, 27.04, 38.49, 45.52, 47.80, 55.79, 62.95, 69.85, and 74.80°. A distinct 2θ value is slightly shifted, which is consistent with JCPDS card 89-1397 (Hosseini and Aboutalebi, 2019). This may confirm the presence of crystalline ZnO embedded within the polymer matrix (Jalal *et al*. 2010).

The poly-4-ATA/TiO_2 composite (Fig. 4e) exhibited diffraction peaks at 23.47, 27.04, 38.68, 45.59, 47.80, 55.79, 61.39, 63.07, 69.73, and 74.86°. Shifts in the 2θ values of 45.59° and 55.79° compared with the pure polymer (45.65 and 55.92) indicate the lattice adjustments due to TiO_2 incorporation. The sharp and intense nature of these reflections shows that TiO_2 crystallites remain intact after integration, as confirmed by JCPDS card 89-6975 (Madhuvilakku and Piraman, 2013).

Among all the composites, TiO_2-based systems display the most intense and well-defined peaks,

indicating superior retention of crystallinity and enhanced ordering within the polymer matrix. By contrast, CeO_2 and ZnO composites introduce greater lattice distortion, producing broader peaks. Thus, TiO_2 incorporation resulted in the highest crystallinity retention compared with the other oxide-loaded systems.

3.4 Electrochemical Impedance Spectra of Poly-4-ATA with Metal Oxides

Figs. 5a–5f show the Nyquist plots obtained from EIS measurements of the bare alloy, poly-4-ATA, and poly-4-ATA coatings incorporated with various metal oxides (SiO_2, CeO_2, ZnO, and TiO_2), while the fitted parameters are listed in Table 3. The charge-transfer resistance (R_{ct}), which represents the resistance to electron exchange between the alloy surface and the electrolyte, was lowest for the uncoated alloy (Fig. 5a), with a value of 1134 Ω cm², confirming its poor corrosion resistance. After applying a poly-4-ATA film (Fig. 5b), the R_{ct} increased to 1.238 × 104 Ω cm², corresponding to an inhibition efficiency of 90.8%, indicating the polymer film provided a protective barrier.

Introducing metal oxides into the polymer matrix further improved the corrosion resistance. The poly-4-ATA/SiO_2 composite (Fig. 5c) exhibited an R_{ct} of 1.791 × 10^4 Ω cm² (IE = 93.6%), suggesting that the silica particles enhanced the protection, though their incomplete dispersion may have limited performance. In poly-4-ATA/CeO_2 (Fig. 5d), R_{ct} increased markedly to 1.811 × 10^4 Ω cm² (IE = 93.7%), pointing to the strong passivating ability of cerium oxide.

Table 3. Impedance parameters for bare Cu–Ni (90/10) alloy, poly-4-ATA and its metal oxide composites

Impedance Parameters	Bare Cu–Ni	Poly-4-ATA	Poly-4-ATA/ SiO_2	Poly-4-ATA/ CeO_2	Poly-4-ATA/ ZnO	Poly-4-ATA/ TiO_2
R_s (Ω cm²)	16.0	15.5	15.0	14.0	11.5	10.2
Q_{dl} (S s^n/cm²)	2.4 x 10^{-4}	8.9 x 10^{-4}	7.5 x 10^{-5}	1.1 x 10^{-4}	5.98 x 10^{-4}	7.53 x 10^{-5}
Q_n	0.8	0.7	0.7	0.6	0.8	0.7
R_{ct} (Ω cm²)	1134	1.238 x 10^4	1.791 x 10^4	1.811 x 10^4	3.458 x 10^4	5.077 x 10^4
Q_f (S s^n/cm²)	-	8.2 x 10^{-5}	5.1 x 10^{-5}	4.8 x 10^{-5}	5.8 x 10^{-5}	8.4 x 10^{-5}
Q_n	-	0.8	0.9	0.9	0.8	0.9
R_f (Ω cm²)	-	187.4	207.3	261.0	270.3	307.9
η (%)	-	90.8	93.6	93.7	96.7	97.8

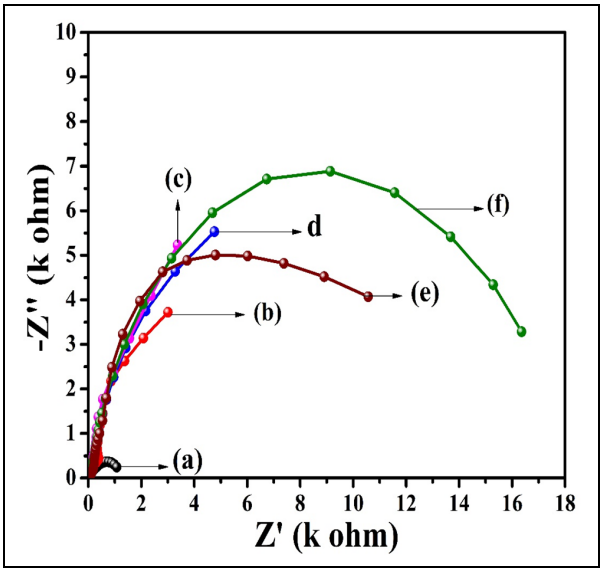


Fig. 5: Nyquist plots of (a) bare Cu–Ni (90/10) alloy, (b) poly-4-ATA, (c) poly-4-ATA/SiO_2, (d) poly-4-ATA/CeO_2, (e) poly-4-ATA/ZnO and (f) poly-4-ATA/TiO_2

The poly-4-ATA/ZnO composite (Fig. 5e) showed an R_{ct} of 3.458 × 10^4 Ω cm² and an inhibition efficiency of 96.7%, which can be attributed to the semiconducting nature of ZnO that suppressed charge transport across the surface.

The better results were obtained with TiO_2 incorporation, where the poly-4-ATA/TiO_2 coating (Fig. 5f) showed an R_{ct} of 5.077 × 10^4 Ω cm² and an inhibition efficiency of 97.8%. This enhanced performance can be linked to the strong interfacial bonding between TiO_2 nanoparticles and the polymer backbone, producing a dense and uniform protective layer that effectively blocks the ingress of corrosive ions.

Overall, the EIS results demonstrated that the embedding of metal oxides into the poly-4-ATA matrix significantly improved the corrosion resistance of Cu–Ni (90/10) alloy, with TiO_2 providing the most effective barrier among the oxides tested.

3.5 Potentiodynamic Polarization Studies of Poly-4-ATA with Metal Oxides

The Tafel polarization curves of poly-4-ATA and its various metal oxide composites are shown in Figs. 6a–6f. The electrochemical parameters extracted from these polarization curves are listed in Table 4. Electrochemical measurements revealed a clear improvement in corrosion resistance upon coating the Cu–Ni alloy with poly-4-ATA and its metal oxide composites.

Table 4. Potentiodynamic polarization values of bare Cu–Ni (90/10) alloy, poly-4-ATA, and its corresponding metal oxides

Electrodes	i_{corr} (µA cm^{-2})	E_{corr} (V vs. SCE)	Inhibition efficiency (%)
Bare Cu–Ni	3.85	-0.23	-
Poly-4-ATA	1.68	-0.27	56.36
Poly-4-ATA/SiO_2	1.23	-0.26	68.05
Poly-4-ATA/CeO_2	0.89	-0.28	76.88
Poly-4-ATA/ZnO	0.46	-0.29	88.05
Poly-4-ATA/TiO_2	0.20	-0.27	94.80

The bare Cu–Ni alloy (Fig. 6a) exhibited a relatively high corrosion current density (i_{corr}) of 3.85 µA cm^{-2}, which indicated active dissolution of the surface in the corrosive environment. After applying poly-4-ATA (Fig. 6b), a considerable reduction in i_{corr} value was observed (1.68 µA cm^{-2}), showing that the polymer layer effectively hindered the corrosion process by forming a protective barrier.

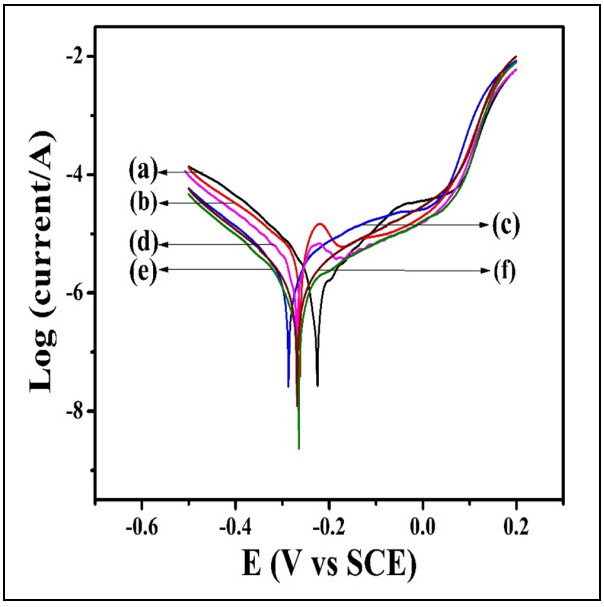


Fig. 6: Tafel polarization plots of (a) bare alloy, (b) poly-4-ATA, (c) poly-4-ATA/SiO_2, (d) poly-4-ATA/CeO_2, (e) poly-4-ATA/ZnO, and (f) poly-4-ATA/TiO_2 in 3.5% NaCl medium

The protective performance was further enhanced when metal oxides were embedded into the polymer matrix. The addition of SiO_2 (poly-4-ATA/SiO_2) and CeO_2 (poly-4-ATA/CeO_2) lowered the i_{corr} value to 1.23 and 0.89 µA cm^{-2}, respectively, as shown in Figs. 6c–d. These oxides likely enhanced the compactness of the film and reduced its porosity, thereby limiting the penetration of aggressive ions. The poly-4-ATA/ZnO composite exhibited a current density of 0.46 µA cm^{-2}, indicating a significant decrease compared with the bare alloy (Fig. 6e), which may be attributed to the semiconducting nature of ZnO that suppressed electron transfer reactions at the metal/electrolyte interface.

The best corrosion protection was achieved with the TiO_2 incorporated (Fig. 6f) polymer, with the lowest i_{corr} value of 0.20 µA cm^{-2}. TiO_2 particles were known for their high stability and strong interaction with polymer chains, leading to a dense and adherent coating that blocks both anodic and cathodic reactions.

The corrosion potential (E_{corr}) values also shifted slightly toward more negative potentials for all the coatings compared with the bare alloy, ranging from −0.23 to −0.29 V vs. the saturated calomel electrode (SCE). This shift suggested the changes in the corrosion mechanism due to the presence of the protective films. Importantly, the inhibition efficiency reached a maximum of 94.80% for the poly-4-ATA/TiO_2 composite, confirming its superior ability to resist corrosion. The incorporation of metal oxides into poly-4-ATA enhanced the overall protective properties of the coatings. The TiO_2-incorporated coating (poly-4-ATA/TiO_2) provided the most effective barrier due to its stability, compatibility with the polymer, and ability to suppress the electrochemical reactions at the surface.

3.6 Atomic Force Microscopy (AFM) Studies of Poly-4-ATA and Poly-4-ATA/TiO_2 Composites

AFM imaging of poly-4-ATA highlights the changes in surface characteristics of the alloy after coating. After applying the poly-4-ATA film (Fig. 7a), the surface becomes more uniform and compact, though some granular patterns are still evident, with the roughness slightly reduced to 215 nm. The same type of surface smooting and reduced rougnes reported in TiO_2 –based nanocomposites coatings (Abilash *et al*. 2025).

The effect is more pronounced in the poly-4-ATA/TiO_2 composite (Fig. 7b), where the surface appears highly compact, continuous, and essentially free of visible flaws, with a significantly lower roughness (Z = 175 nm). The introduction of TiO_2 nanoparticles improved chain packing within the polymer, minimized voids, and produced a smoother topography. This structural refinement supports the electrochemical observations, showing that the TiO_2-containing composite provides the maximum corrosion resistance (97.8%). Collectively, the AFM analysis confirmed that oxide incorporation enhanced the barrier properties and markedly improved the protective efficiency of the coating.

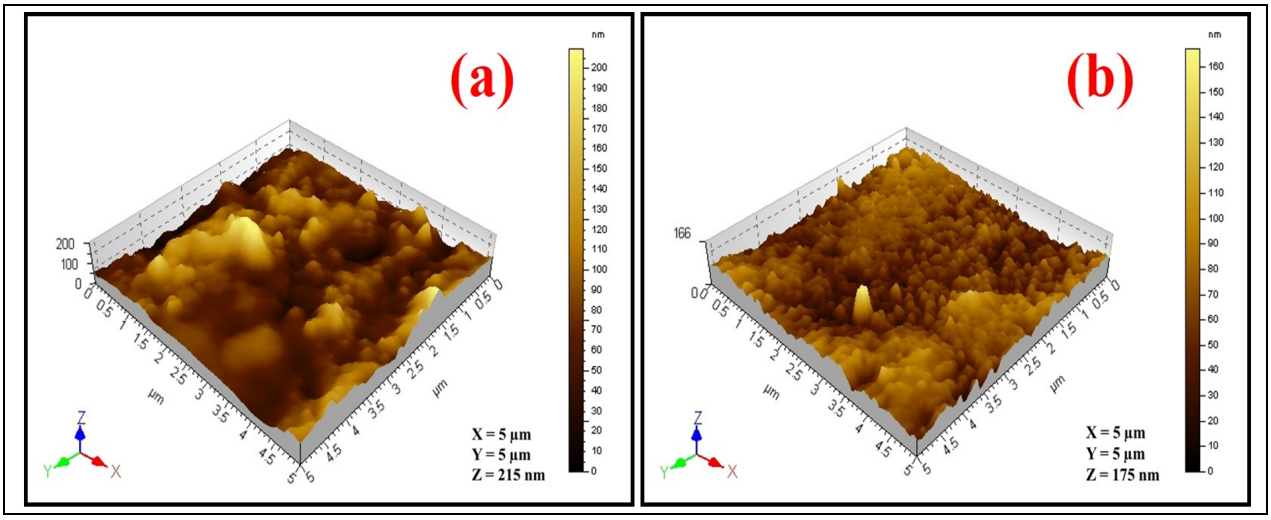


Fig. 7: AFM images of (a) poly-4-ATA and (b) poly-4-ATA/TiO_2

3.7 SEM Analysis of Poly-4-ATA with Metal Oxide Composites

SEM analysis was carried out to compare the surface features of the uncoated Cu–Ni alloy, the poly-4-ATA layer, and the poly-4-ATA with metal oxide composites (Fig. 8). The bare alloy (Fig. 8a) displayed grooves and irregular marks, showing the typical texture of an exposed metallic surface that can be readily attacked in aggressive environments. After deposition of poly-4-ATA (Fig. 8b), the surface was partially masked by a polymer layer, although small uneven regions and micro-scale defects remained, which could still act as sites for localized degradation.

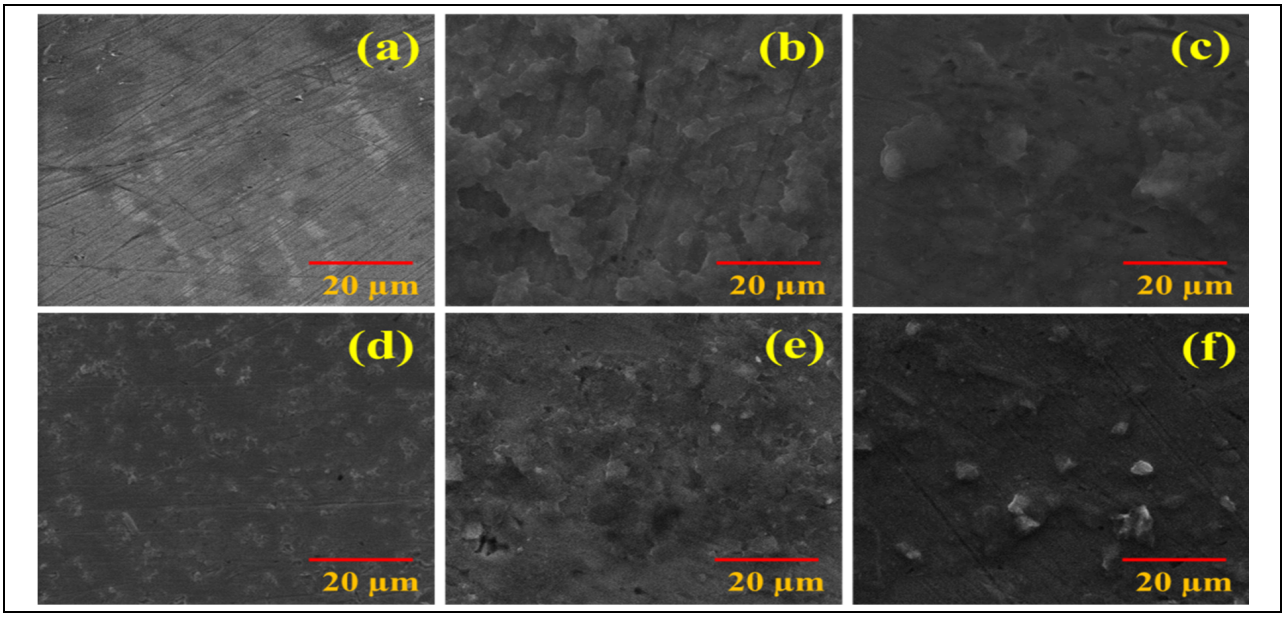


Fig. 8: SEM images of (a) bare Cu–Ni (90/10) alloy, (b) poly-4-ATA, (c) poly-4-ATA/SiO_2, (d) poly-4-ATA/CeO_2, (e) poly-4-ATA/ZnO, and (f) poly-4-ATA/TiO_2

Incorporation of SiO_2 (Fig. 8c) produced a comparatively smooth and uniform film, indicating a good level of oxide dispersion in the matrix of poly-4-ATA/SiO_2 composite. The CeO_2 composite of poly-4-ATA/CeO_2 (Fig. 8d) showed a more compact granular appearance, suggesting strong particle–polymer contact, which enhanced the barrier capacity of the coating. In the case of poly-4-ATA/ZnO (Fig. 8e), dispersed ZnO clusters were embedded within the coating, giving localized reinforcement but also leading to slight surface roughness. The TiO_2-filled system (Fig. 8f) exhibited a dense, continuous, and defect-free layer, reflecting superior oxide distribution and strong interfacial compatibility with the host polymer.NANO

The morphologies observed for each system support the electrochemical measurements, with the TiO_2 composite delivering the best protection (97.8%

efficiency) due to its compact structure and improved adherence, which restricts electrolyte penetration and delays corrosion.

3.8 Energy-Dispersive X-ray Analysis (EDAX) of Poly-4-ATA with Metal Oxide Composites

Fig. 9 illustrates the EDAX spectrum recorded for the poly-4-ATA coating on the Cu–Ni alloy. The spectrum showed signals at approximately 0.25 keV and 0.4 keV, corresponding to carbon and nitrogen, which confirmed the incorporation of poly-4-ATA. The strong peaks noticed at ~7.5 keV and ~8 keV are characteristic of nickel and copper originating from the alloy substrate. In addition, weaker signals associated with oxygen (~0.5 keV), sodium (~1 keV), manganese (~0.65 keV), and iron (~0.7 and 6.4 keV) were present, which could be attributed to trace-level impurities within the Cu–Ni alloy (90/10).

Figs. 10a–10d illustrate the EDAX spectra of poly-4-ATA combined with SiO_2, CeO_2, ZnO and TiO_2 to produce the poly-4-ATA/SiO_2, poly-4-ATA/CeO_2, poly-4-ZnO and poly-4-ATA/TiO_2, respectively. The elemental peaks were observed for silicon at ~1.8 keV (Fig. 10a), cerium at ~0.9 and 4.8 keV (Fig. 10b), zinc at ~1.0 and 8.5 keV (Fig. 10c), and titanium at ~0.4 and 4.5 keV (Fig. 10d).

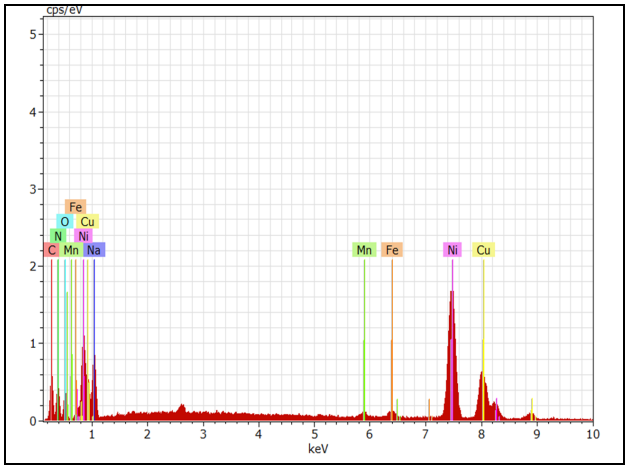


Fig. 9: EDAX spectrum of poly-4-ATA with Cu–Ni (90/10) alloy

The presence of these signals confirmed the successful incorporation of the respective metal oxides into the poly-4-ATA matrix. Importantly, the appearance of well-defined oxide peaks indicated that these species were not simply deposited on the surface but were strongly interconnected with the polymer framework. Such incorporation was expected to enhance the stability, conductivity, and overall electrochemical behavior of the composites, rendering them suitable as protective coatings in Cu–Ni (90/10) alloy.

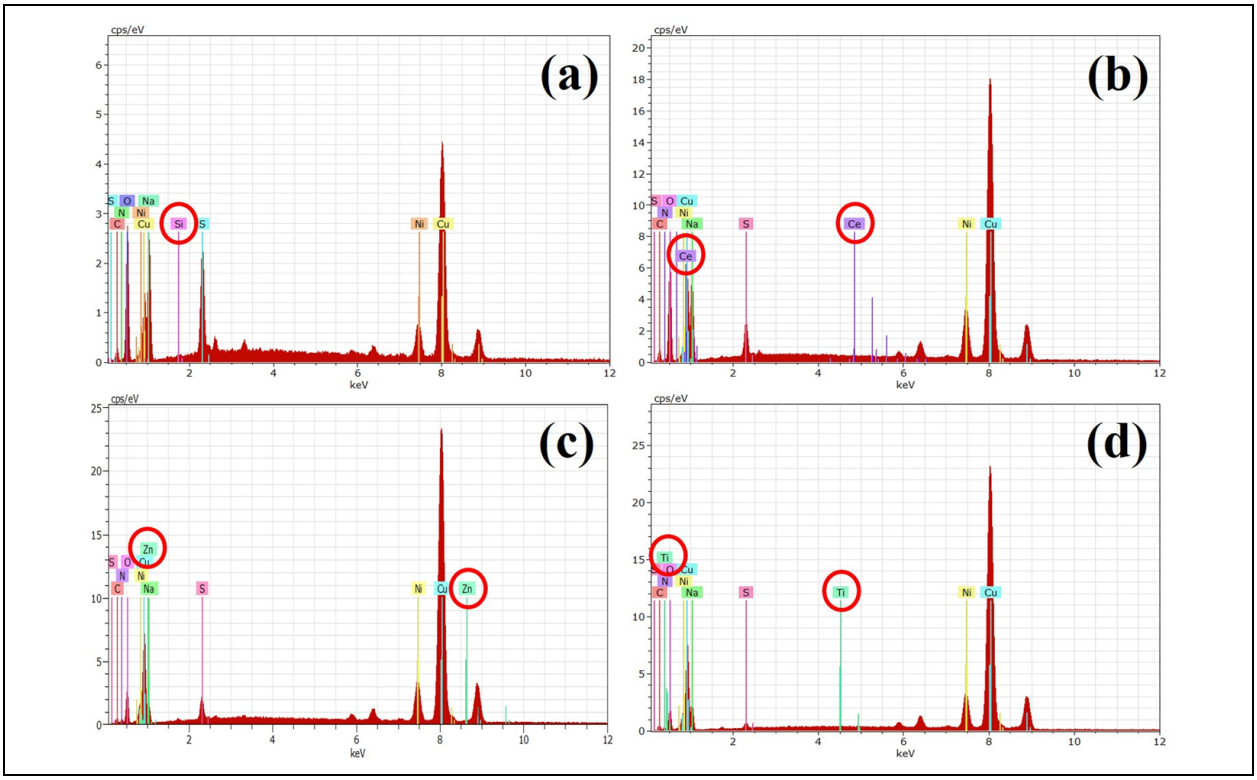


Fig. 10: EDAX spectra of (a) poly-4-ATA/SiO_2, (b) poly-4-ATA/CeO_2, (c) poly-4-ATA/ZnO, and (d) poly-4-ATA/TiO_2

4. CONCLUSION

The successful fabrication of poly(4-amino-1,2,4-triazole) composites with various inorganic metal oxides was confirmed through structural, morphological, and electrochemical analyses. FT-IR spectra verified the interactions between the polymer matrix and the metal oxide particles, while XRD patterns indicated partial crystallinity resulting from the oxide incorporation. SEM images revealed a uniform, compact surface morphology with reduced porosity compared to the pure polymer, and EDAX analysis confirmed the presence of silicon, cerium, zinc, and titanium, which were effectively embedded in the metal oxide–polymer network. EIS demonstrated a substantial increase in charge-transfer resistance, reflecting an enhanced barrier effect against electrolyte penetration. Potentiodynamic polarization results further showed a significant reduction in corrosion current density (i_{corr}), highlighting the superior inhibition efficiency of the composite coating. Collectively, these findings establish that the synergistic combination of poly-4-ATA with the TiO_2 composite exhibits the highest inhibition efficiency for the Cu–Ni (90/10) alloy in chloride media. This composite represents a promising candidate for advanced protective coatings in aggressive environments.

FUNDING

This research received no specific grant from any funding agency in the public, commercial, or not-for-profit sectors.

CONFLICTS OF INTEREST

The authors declare that there is no conflict of interest.

COPYRIGHT

This article is an open-access article distributed under the terms and conditions of the Creative Commons Attribution (CC BY) license (http://creativecommons.org/licenses/by/4.0/).

REFERENCES

Abilash, R., Muraliraja R. and Shasisundaram V. S.,Electroless Ni-P-TiO_2 nanocomposite coatings for enhanced durability and saltwater corrosion protection of jet ski engine components, *J.Enviorn. Nanotechnol.*, 14(3), 685-691(2025), https://doi.org/10.13074/jent.2025.09.2531734

Akpan, E. D., Singh, A. K., Lgaz, H., Quadri, T. W., Shukla, S. K., Mangla, B., Dwivedi, A., Dagdag, O., Sheetal, Inyang, E. E. and Ebenso, E. E., Coordination compounds as corrosion inhibitors of metals: A review, *Coord. Chem. Rev*., 499, 215503 (2024). https://doi.org/10.1016/j.ccr.2023.215503

Aslam, R., Mobin, M., Zehra, S. and Aslam, J., A comprehensive review of corrosion inhibitors employed to mitigate stainless steel corrosion in different environments, *J. Mol. Liq.,* 364, 119992 (2022). https://doi.org/10.1016/j.molliq.2022.119992

Ates, M., Kalender, O., Topkaya, E. and Kamer, L., Polyaniline and polypyrrole/TiO_2 nanocomposite coatings on Al1050: electrosynthesis, characterization and their corrosion protection ability in saltwater media, *Iran. Polym. J.,* 24(7), 607–619 (2015). https://doi.org/10.1007/s13726-015-0352-1

Aydın, F., A review of recent developments in the corrosion performance of aluminium matrix composites, *J. Alloys Compd.,* 949, 169508 (2023). https://doi.org/10.1016/j.jallcom.2023.169508

Choudhury, B. and Choudhury, A., Ce^{3+} and oxygen vacancy mediated tuning of structural and optical properties of CeO_2 nanoparticles, *Mater. Chem. Phys.,* 131, 666–671 (2012). https://doi.org/10.1016/j.matchemphys.2011.10.032

Edison, T. N. J. I., Atchudan, R., Pugazhendhi, A., Lee, Y. R. and Sethuraman, M. G., Corrosion inhibition performance of spermidine on mild steel in acid media, *J. Mol. Liq.,* 264, 483–489 (2018). https://doi.org/10.1016/j.molliq.2018.05.087

Elangovan, N., Srinivasan, A., Pugalmani, S., Kalaiyarasan, M., Rajendran, N., Seikh, A. H. and Rajendiran, N., Development and electrochemical investigations of enhanced corrosion-resistant polyvinylcarbazole-TiO_2 hybrid nanocomposite coatings on 316L SS for marine applications, *Surf. Coatings Technol.,* 481, 130628 (2024). https://doi.org/10.1016/j.surfcoat.2024.130628

Hosseini, M. G. and Aboutalebi, K., Enhancement of anticorrosive resistance of epoxy coatings by incorporation of CeO_2@polyaniline@2-mercaptobenzothiazole nanocomposite, *Synth. Met*., 250, 63–72 (2019). https://doi.org/10.1016/j.synthmet.2019.03.001

Jalal, R., Goharshadi, E. K., Abareshi, M., Moosavi, M., Yousefi, A. and Nancarrow, P., ZnO nanofluids: Green synthesis, characterization, and antibacterial activity, *Mater. Chem. Phys*., 121, 198–201 (2010). https://doi.org/10.1016/j.matchemphys.2010.01.020

Li, L., Liu, L., Li, Z., Hu, D., Gao, C., Xiong, J. and Li, W., The synthesis of CB[8]/ZnO composite materials with enhanced photocatalytic activities, *Heliyon*, 5(5), e01714 (2019). https://doi.org/10.1016/j.heliyon.2019.e01714

Madhuvilakku, R. and Piraman, S., Biodiesel synthesis by TiO_2–ZnO mixed oxide nanocatalyst catalyzed palm oil transesterification process, *Bioresour. Technol.,* 150, 55–59 (2013). https://doi.org/10.1016/j.biortech.2013.09.087

Mohanty, A., Kumar, S. and Tiwari, S. K., Assessment of N-(4H-1,2,4-triazol-4-yl) octanamide as hydrochloric acid corrosion inhibitor for mild steel, *Mater. Today Commun*., 27, 102439 (2021). https://doi.org/10.1016/j.mtcomm.2021.102439

Phadke, S. N., Alva, V. D. P. and Samshuddin, S., A Review on 1,2,4-Triazole Derivatives as Corrosion Inhibitors, *J. Bio-Tribo-Corrosion*, 3, 1–12 (2017). https://doi.org/10.1007/s40735-017-0102-3

Rajkumar, G. and Sethuraman, M. G., Electrochemical synthesis of poly-3-amino-5-mercapto-1,2,4-triazole on copper and its protective effect in 3.5 % NaCl medium, *Res. Chem. Intermed*., 41, 8041–8055 (2015). https://doi.org/10.1007/s11164-014-1876-2

Rajkumar, G. and Sethuraman, M. G., Synthesis, characterization and corrosion protection of poly-4-methyl-3-mercapto-1,2,4-triazole/TiO_2 composite on copper, *Polym. Bull*., 71(12), 3249–3260 (2014). https://doi.org/10.1007/s00289-014-1248-5

Saravanan, S. and Dubey, R. S., Synthesis of SiO_2 nanoparticles by sol–gel method and their optical and structural properties, *Rom. J. Inf. Sci. Technol.,* 23(1), 105–112 (2020).

Singh, J., Sahu, K., Satpati, B. and Mohapatra, S., Facile synthesis, structural, optical and photocatalytic properties of anatase/rutile mixed-phase TiO_2 ball-like sub-micron structures, *Optik (Stuttg).,* 188, 270–276 (2019). https://doi.org/10.1016/j.ijleo.2019.05.053

Vinothkumar, K. and Sethuraman, M. G., A robust method of enhancement of corrosion inhibitive ability of electrodeposited poly-3-amino-5-mercapto-1,2,4-triazole films over copper surface using graphene oxide, *J. Adhes. Sci. Technol*., 34(6), 651–669 (2020). https://doi.org/10.1080/01694243.2019.1674599

Vinothkumar, K. and Sethuraman, M. G., Corrosion inhibition ability of electropolymerised composite film of 2-amino-5-mercapto-1,3,4-thiadiazole/TiO_2 deposited over the copper electrode in neutral medium, *Mater. Today Commun*., 14, 27–39 (2018). https://doi.org/10.1016/j.mtcomm.2017.12.007

Winkler, D. A., Hughes, A. E., Özkan, C., Mol, A., Würger, T., Feiler, C., Zhang, D. and Lamaka, S. V., Impact of inhibition mechanisms, automation, and computational models on the discovery of organic corrosion inhibitors, *Prog. Mater. Sci.,* 149, 101392 (2025). https://doi.org/10.1016/j.pmatsci.2024.101392